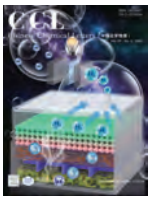
Chinese Chemical Letters 37 (2026) 111630

Contents lists available at ScienceDirect

Chinese Chemical Letters

journal homepage: www.elsevier.com/locate/cclet



Molybdenum pentaboride mediated direct and indirect approaches for boosting Fenton-like activation of peroxymonosulfate towards water decontamination

Xinyun Zhang[a,b], Chenying Zhou[a,b], Jian Zhang[c], Minglu Sun[a,b,*], Yanbiao Shi[a,b], Chuanshu He[a,b], Xiaowei Huo[d], Yang Liu[a,b], Peng Zhou[a,b,*], Bo Lai[a,b]

[a] State Key Laboratory of Hydraulics and Mountain River Engineering, College of Architecture and Environment, Sichuan University, Chengdu 610065, China
[b] Sino-German Centre for Water and Health Research, Sichuan University, Chengdu 610041, China
[c] Sichuan Development Environmental Science and Technology Research Institute Co., Ltd., Chengdu 610095, China
[d] China Construction Third Engineering Bureau Group Southwest Co., Ltd., Chengdu 610200, China

ARTICLE INFO

Article history:
Received 13 June 2025
Revised 16 July 2025
Accepted 23 July 2025
Available online 24 July 2025

Keywords:
Molybdenum pentaboride
Peroxymonosulfate
Fenton-like oxidation
Reactive oxygen species
Fe(III)/Fe(II) circulation

ABSTRACT

The Fenton-like activation of peroxymonosulfate (PMS) is an effective oxidation strategy for water decontamination, however, Fe(II)-mediated Fenton-like reactions suffer from limitations of sluggish iron species cycling and iron sludge accumulation. Herein, molybdenum pentaboride (Mo_2B_5) was innovatively employed as a dual-functional co-catalyst to address these challenges *via* synergistically direct and indirect routes for activating PMS. Mo_2B_5 can promptly enhance Fe(III)/PMS to entirely degrade sulfamethoxazole within 4 min, superior to conventional reducing agents and carbon-based co-catalysts. Based on mechanism investigations (reactive oxygen species analysis, iron species variation, surface chemistry characterizations), the distinctive electronic configuration of Mo_2B_5 can direct activate PMS for generating hydroxyl radical ($^{\bullet}OH$), while simultaneously enhance Fe(II) regeneration to facilitate subsequent Fenton-like processes to produce sulfate radicals ($SO_4^{\bullet-}$) and ferryl species (Fe(IV)). The system thus demonstrated broad applicability for degrading diverse pollutants with high rate constants, while the substrate specific reactivities are dependent on the electron-donating capacities of pollutants. In addition, Mo_2B_5 exhibits exceptional stability over consecutive cycle tests, attributed to its self-cleaning surface and retained crystallinity.

© 2026 Published by Elsevier B.V. on behalf of Chinese Chemical Society and Institute of Materia Medica, Chinese Academy of Medical Sciences.

Advanced oxidation technologies have the advantages of fast kinetic rates and high degrading efficiency, making them potential methods for eliminating stubborn pollutants for environmental remediation [1]. This catalytic mechanism can generate diverse reactive oxygen species (ROS), predominantly hydroxyl ($^{\bullet}OH$) and sulfate ($SO_4^{\bullet-}$) radicals by efficient peroxymonosulfate (PMS) activation [2], while $SO_4^{\bullet-}$ exhibits superior persistence and enhanced contaminant selectivity compared to $^{\bullet}OH$ [3]. In general, Fe(II) as an eco-friendly catalyst mediated Fenton-like mechanism is an effective route for activating PMS, it has also been widely selected in research reports for activating PMS and initiation of Fenton-like catalytic cycles (Eqs. 1–3) [4,5]. Nevertheless, the slow Fe(III) reduction kinetics lead to rapid iron accumulation, which can significantly restrict sustained ROS generation.

Consequently, various approaches have been developed to optimize the iron species cycle, thereby enhancing Fenton-like PMS activation through the incorporation of external physical stimuli and co-catalytic components [6]. While external stimuli (*e.g.*, electrolysis, photolysis, and thermal activation) can mitigate Fe(III) accumulation, they often suffer from energy-intensive operations, elevated costs, and complex instrumentations [7]. Iron-chelating organic ligands (*e.g.*, pyridine carboxylic acid [8]) and electron-donating compounds (*e.g.*, L-cysteine [9] and human acid [10]) widely serve as energy-efficient promoters for Fe(II) regeneration [11]. Nevertheless, the application of these organic promoters may lead to secondary environmental contamination owing to their limited recyclability and inherent toxicity, while the scavenging effect for ROS induced by homogeneity will cause low removal efficiency of target pollutants. In recent years, metal sulfides (*e.g.*, WS_2 and MoS_2 [12]) and carbonaceous materials (*e.g.*, nitrogen-doped carbon nanotube [13] and graphene [14]) have been increasingly used to facilitate Fenton-like chemistry. However, the risk of formation

* Corresponding authors.
E-mail addresses: sunminglu27@163.com (M. Sun), zhoup1219@sina.com (P. Zhou).

https://doi.org/10.1016/j.cclet.2025.111630
1001-8417/© 2026 Published by Elsevier B.V. on behalf of Chinese Chemical Society and Institute of Materia Medica, Chinese Academy of Medical Sciences.

of surface passivation layer and low iron cycling efficiency strongly limit their applications. Accordingly, seeking for long-lasting and environmentally friendly electron sacrificers is paramount for developing sustainable PMS-based Fenton-like techniques.

$$Fe(II) + HSO_5^- \rightarrow Fe(IV) + SO_4^{2-} + H^+ \quad (1)$$

$$Fe(II) + HSO_5^- \rightarrow Fe(III) + SO_4^{\bullet-} + OH \quad (2)$$

$$SO_4^{\bullet-} + OH^- \rightarrow SO_4^{2-} + {}^{\bullet}OH \quad (3)$$

Molybdenum pentaboride (Mo_2B_5) has great potential in enhancing Fenton-like reactions [15]. Boron atom has a specific electron configuration ($1s^2 2s^2 2p^1$) [16], the outermost layer of boron does not reach a sTable 8-electron configuration and is thus in an electron-deficient state. This electron deficient property endows boron with Lewis acidity, allowing it to accept electron pairs and form coordination adsorption with negatively charged groups, such as the O–O or S-O of PMS molecule. In addition, the electronic configuration of molybdenum is $[Kr]4d^5 5s^1$, with abundant d-orbital electrons that can flexibly undergo oxidation state changes from +2 to +6. The molybdenum atom of Mo_2B_5 usually exists in the +3 and may directly provide electrons for initiating Fe(III) reduction as an electron donor [17]. Meanwhile, the boron and molybdenum in lower oxidation states on Mo_2B_5 surfaces facilitate efficient electron transfer to ferric species (*e.g.*, Fe^{3+} and $FeOH^{2+}$) [18]. This electron donation process may accelerate ferrous ions regeneration, thereby enhancing the kinetics of the rate-determining step in Fenton-like catalytic cycles [19]. Therefore, Mo_2B_5 also has great potential in indirectly activating PMS to produce ROS, and meanwhile, low valence molybdenum and boron form a co-catalyst with dual reduction sites for promoting Fe(III) reduction. In addition, Mo_2B_5, a cost-effective metal boride composed of abundant natural elements, is typically prepared by straightforward solid-phase reactions involving molybdenum metal and amorphous boron [20]. Thus, Mo_2B_5 is a promising co-catalyst with high conductivity and cost-effectiveness of dual reduction sites to facilitate direct and indirect activation of PMS [7,21,22].

In this study, Mo_2B_5 was used as a co-catalyst to enhance PMS activation *via* dual reaction pathways for accelerating the production of ROS and degrading organic pollutants, with sulfamethoxazole (SIZ) serving as the model contaminant. The co-catalytic performance of Mo_2B_5 was compared with common solid co-catalysts (carbon materials (CNT, Graphite, WC, Biochar, rGO), metallic species in the zero valent state (W and Mo), metal sulfides (WS_2 and MoS_2), metal borides (ZrB_2, CrB_2, CaB_6, FeB_2, TiB_2, HfB_2, NbB_2, VB_2, MoB, Co_2B, WB), phosphorus (P), and dissolved reducing agents (ascorbic acid (AA), hydroquinone (HQ), L-cysteine (L-CE), sodium sulfite (SS)). In addition, the identification and quantification of ROS were systematically investigated through an integrated approach incorporating radical scavenging experiments, chemical probe methodologies, electron paramagnetic resonance (EPR) tests as well as substrate specific reactivity analysis. The co-catalytic mechanisms of Mo_2B_5 for assisting Fe(III)/PMS were investigated and clarified comprehensively based on the analysis of iron transformation and characterizations (X-ray photoelectron spectroscopy (XPS), X-ray diffraction (XRD), high resolution transmission electron microscopy (HRTEM), Raman spectroscopy, and Fourier transform infrared spectroscopy (FT-IR)) of Mo_2B_5. The details of materials and methods were shown in Text S1-S8 (Supporting information).

The co-catalytic effects of Mo_2B_5 on both Fe(III)/PMS and Fe(II)/PMS were systematically investigated. Fig. 1a depicts PMS system cannot directly degrade SIZ, but the Mo_2B_5/PMS system degraded 18 % of SIZ at 15 min. It is shown that Mo_2B_5 consisting of the transition metal molybdenum and the semi-metallic element boron [7,23] can effectively and directly activate PMS to generate ROS for SIZ degradation. The unique activation ability of Mo_2B_5 for PMS stems from the precise matching of the dual active sites of Mo and B on its surface with the asymmetric molecular structure of PMS. Compared to the symmetrically structured peroxydisulfate and hydrogen peroxide, the asymmetric O–O bond of PMS is more susceptible abnormal fracture on the surface of Mo_2B_5 for direct electron transfer from Mo_2B_5 to PMS [24]. Moreover, Fe(III) could not effectively activate PMS to eliminate SIZ (<3 %), whereas Fe(II) can effectively activate PMS to degrade SIZ (22 %) *via* Fe(II) induced cleavage of O–O bond of PMS (Fig. 1b). The low degradation rate of SIZ by Fe(II)/PMS indicates that SIZ was degraded

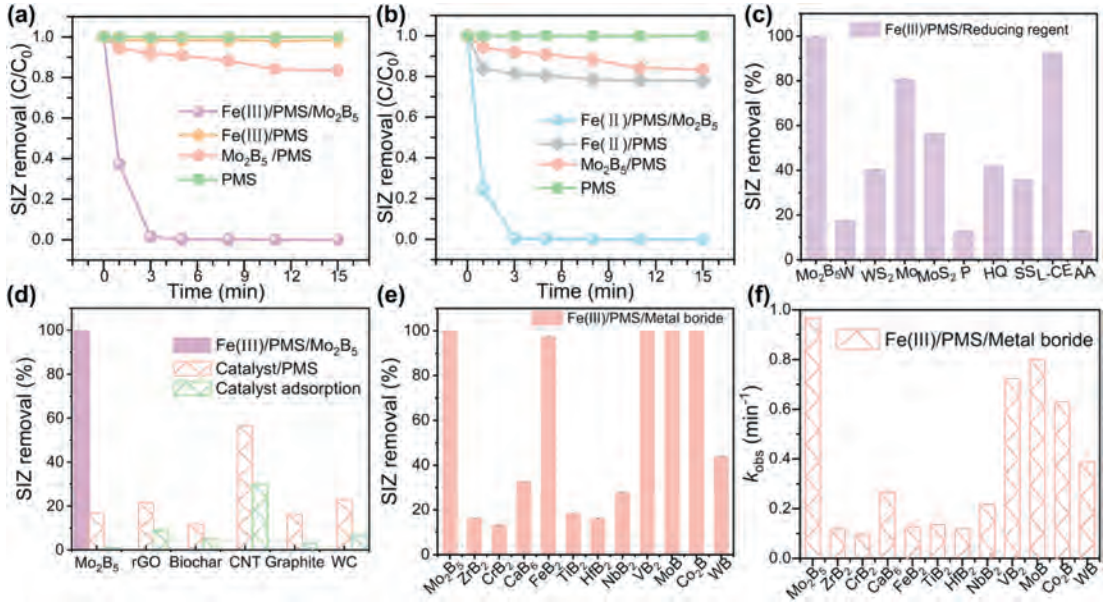


Fig. 1. Co-catalytic activity of Mo_2B_5 for enhancing Fe(III)/PMS system. Mo_2B_5 assisted (a) Fe(III)/PMS and (b) Fe(II)/PMS. (c) Reducing agents assisted Fe(III)/PMS and (d) direct activation of PMS by carbon materials. Various metal brides assisted Fe(III)/PMS for (e) ratios and (f) k_{obs} of SIZ removal.

in the first stage within 2 min. The rapid accumulation of Fe(III) coupled with inefficient Fe(II) regeneration significantly constrains sustained SIZ degradation during secondary reaction phases [25]. When Mo_2B_5 was used as a co-catalyst in Fenton-like reaction, it significantly contributed to the oxidation capability of Fe(III)/PMS and Fe(II)/PMS, while SIZ was fully degraded within 4 min in both systems. Thus, Mo_2B_5 as a co-catalyst can directly activate PMS to produce ROS and simultaneously promote iron redox cycling to accelerate Fenton-like oxidation. The superior stability of Fe(III) relative to Fe(II) makes it more appropriate for further mechanistic study in Mo_2B_5 co-catalyzed Fenton-like systems. The performance of Fe(III)/Mo_2B_5/PMS is pH-dependent, which exhibited optimal efficiency for degrading SIZ at pH 3.0 (Fig. S1 in Supporting information).

Then, a wide spectrum of co-catalysts were applied for assisting Fenton-like activation of PMS by comparing with Mo_2B_5. The results in Fig. 1c and Fig. S2 (Supporting information) indicate that Mo_2B_5 (100 %) outperformed than other reducing agents (W (18 %), WS_2 (41 %), Mo (81 %), MoS_2 (57 %), P (13 %), HQ (42 %), SS (36 %), L-CE (93 %), and AA (13 %)) for promoting Fe(III)/PMS to remove SIZ. Previous literature reported that carbon materials mediated activation of PMS can also significantly degrade organic contaminants [26], thus, we compared the performance of Mo_2B_5/Fe(III)/PMS with various carbon materials assisted PMS systems [27,28]. Fig. 1d and Fig. S3 (Supporting information) show that rGO, CNT, Graphite, Biochar, and WC coupled PMS systems only degraded 22 %, 12 %, 57 %, 16 %, and 23 % of SIZ at 15 min, respectively, which are markedly lower than that in Mo_2B_5/Fe(III)/PMS. Moreover, the reactivities of these carbon materials as co-catalysts of Fe(III)/PMS were also markedly lower than that of Mo_2B_5 (Fig. S4 in Supporting information). Although the performance of Mo_2B_5 in directly activating PMS is not prominent, the performance of Mo_2B_5/Fe(III)/PMS is superior to carbon material assisted systems. In recent years, the effective enhancement of the catalytic activity of carbon materials for PMS activation were widely investigated by defect engineering and surface modifications (*e.g.*, surface functional groups and heteroatom doping) [29]. However, carbon materials assisted PMS systems only exhibit high activity in degrading organic compounds with electron-rich groups, while Mo_2B_5 shows higher co-catalytic efficiency and wider adaptability for diverse organic contaminants [29–32]. In addition, various metal borides (ZrB_2, CrB_2, CaB_6, FeB_2, TiB_2, HfB_2, NbB_2, VB_2, MoB, Co_2B, WB) also demonstrated capability in enhancing Fe(III)/PMS (Fig. 1e and Fig. S5 in Supporting information), and meanwhile, Mo_2B_5 exhibited superior co-catalytic performance compared with other metal borides. Benchmarking experiments demonstrated the 1.2–10.1 times higher k_{obs} for SIZ removal (0.97 min^{-1}) in Mo_2B_5/Fe(III)/PMS compared to alternative metal boride co-catalysts assisted systems (Fig. 1f and Text S9 in Supporting information). The exceptional co-catalytic behavior of Mo_2B_5 is mechanistically attributed to its optimized electronic structure and abundant surface active sites, which may synergistically facilitate (1) direct PMS activation and (2) stabilized Fe(III)/Fe(II) redox cycling for indirect Fenton-like reaction (Fig. S6 in Supporting information).

Previous reports indicated that PMS decomposition catalyzed by iron can generate multiple ROS [33,34]. As depicted in Fig. 2a and Fig. S7 (Supporting information), comparing with extremely low PMS decomposition in Fe(III)/PMS, the PMS depletion in Mo_2B_5/PMS is 0.15 mmol/L at 15 min, which implies the capability of Mo_2B_5 to directly decompose PMS. The Mo_2B_5/Fe(III)/PMS system consumed 0.45 mmol/L PMS at 15 min, indicating that Mo_2B_5 can significantly promote indirect decomposition of PMS for ROS formation *via* Fenton-like reaction. The generated ROS were thus *in-situ* characterized through EPR tests using DMPO as the chemical probe (Fig. 2b and Fig. S8 in Supporting information).

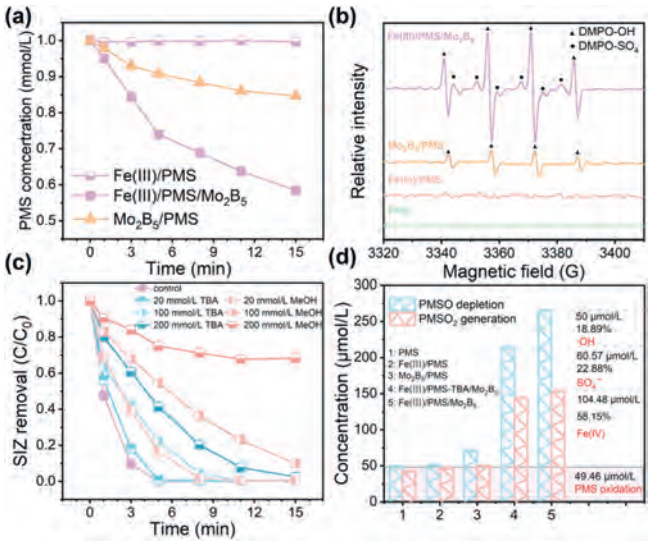


Fig. 2. Identification of various ROS in the Mo_2B_5/Fe(III)/PMS system. (a) PMS consumption, (b) EPR spectra, (c) quenching tests, (d) contributions of different ROS for PMSO oxidation.

formation). EPR spectrum revealed no detectable DMPO-radical adduct in Fe(III)/PMS, confirming the limited capacity of Fe(III) for direct PMS activation. The detection of DMPO–OH adducts ($\alpha^N = \alpha^H = 14.9$ G, with 1:2:2:1 quartet peak intensity ratio) in Mo_2B_5/PMS provides conclusive evidence that Mo_2B_5 can directly activate PMS and promote O–O bond cleavage for producing $^{\bullet}OH$ rather than $SO_4^{\bullet-}$ [35]. Moreover, the EPR spectra revealed significantly enhanced DMPO–OH adduct signal in Mo_2B_5/Fe(III)/PMS compared to Mo_2B_5/PMS, accompanied by characteristic DMPO-SO_4 peaks ($\alpha^H = 0.75$ G, 1.42 G, 10.1 G; $\alpha^N = 13.7$ G) [36]. These observations unveil the capability of Mo_2B_5 to promote Fe(III)/Fe(II) redox cycling, thereby facilitating indirect generation of reactive radicals ($SO_4^{\bullet-}$ and $^{\bullet}OH$) in Fenton-like process. Moreover, quenching tests employing *tert*–butyl alcohol (TBA) and methanol (MeOH) as radical quenchers for selectively scavenging $^{\bullet}OH$ and $SO_4^{\bullet-}$ in Mo_2B_5/Fe(III)/PMS were carried out, resulting from the distinct rate constants of MeOH and TBA for reacting with $SO_4^{\bullet-}$ and $^{\bullet}OH$ [37,38]. Fig. 2c clearly illustrates the differential inhibition effects of MeOH and TBA, MeOH reduced the degradation efficiency by 56 %, whereas TBA caused a comparatively lower inhibition of 22 %. The significant suppression by TBA confirms the non-negligible contribution of $^{\bullet}OH$, whereas the higher inhibition ratio by MeOH suggests concurrent involvement of $SO_4^{\bullet-}$. The result demonstrated that both $^{\bullet}OH$ and $SO_4^{\bullet-}$ participate in SIZ oxidation. In addition, EPR analysis of Mo_2B_5/Fe(III)/PMS also revealed the presence of singlet oxygen ($^1O_2$, Fig. S9 in Supporting information), while superoxide radical was not detected (Fig. S10 in Supporting information), indicating that Mo_2B_5 can mediate energy transfer to generate $^1O_2$. Nevertheless, considering the indistinctive inhibition effect of sugar alcohol on SIZ degradation (Fig. S9) and the non-negligible scavenging effect of sugar alcohol on $^{\bullet}OH$ and $SO_4^{\bullet-}$, $^1O_2$ induced SIZ removal in Mo_2B_5/Fe(III)/PMS is not the dominant approach.

Moreover, current scientific discussion propose that Fe(II) may facilitate heterolytic dissociation of peroxide bond in PMS to produce Fe(IV) under acidic condition [39]. The limited reaction kinetics among Fe(IV) and scavengers ($k_{(MeOH)} = 571$ L mol^{-1} s^{-1}, $k_{(TBA)} = 60$ L mol^{-1} s^{-1}) suggest the potential Fe(IV) formation in Mo_2B_5/Fe(III)/PMS, as evidenced by significant SIZ degradation (32 %) with high dosage of MeOH for scavenging $SO_4^{\bullet-}$ and $^{\bullet}OH$ (Fig. 2c) [22,40]. The present study investigated the role of Fe(IV) in Mo_2B_5/Fe(III)/PMS *via* methyl phenyl sulfoxide (PMSO)-based

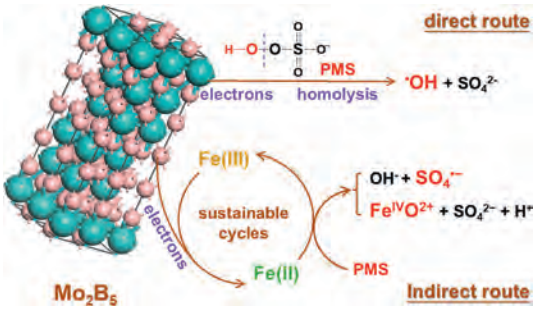


Fig. 3. The routes of the Mo_2B_5/Fe(III)/PMS system for producing ROS.

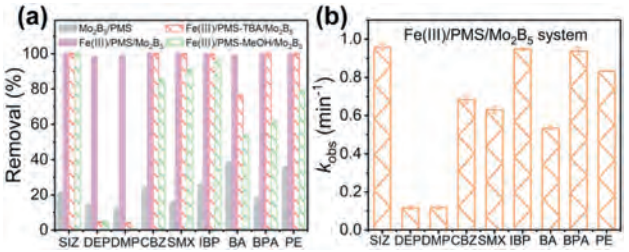


Fig. 4. (a) Efficiencies and (b) k_{obs} for degrading multiple pollutants in the Mo_2B_5/Fe(III)/PMS system.

probe experiments, enabling both qualitative and semi-quantitative determination of Fe(IV) generation while differentiating between radical ($SO_4^{\bullet-}$ and $^{\bullet}OH$) and non-radical (Fe(IV)) oxidation pathways. This result can be attributed to the unique oxygen transfer mechanism of Fe(IV), which can selectively oxidize sulfoxides to their corresponding sulfones [41]. Fig. 2d reveals that Fe(IV) contributes obviously to PMSO oxidation in Mo_2B_5/Fe(III)/PMS, exhibiting a $PMSO_2$ yield of 58 % relative to PMSO consumption (105 μmol/L). These experimental findings substantiate that Fe(IV) can serve as a crucial ROS for degrading organic pollutants. Moreover, by adding TBA into Mo_2B_5/Fe(III)/PMS for selectively terminating $^{\bullet}OH$ induced oxidation of PMSO, it was found that $^{\bullet}OH$ and $SO_4^{\bullet-}$ contributed to 19 % and 23 % of PMSO degradation, respectively. Thus Mo_2B_5/Fe(III)/PMS can synergistically degrade organic pollutants through combined radical ($SO_4^{\bullet-}$ and $^{\bullet}OH$) and non-radical (Fe(IV)) pathways. Due to the generation of multiple ROS for degrading organic pollutants *via* synergetic radical and non-radical routes, the system coupling Mo_2B_5 and Fe(III)/PMS immunes largely from various anions (Cl^-, SO_4^{2-}, NO_3^- and HCO_3^-, Fig. S11 in Supporting information).

The combined results from EPR, radical screening, and PMSO chemical probe collectively unveil that Mo_2B_5/Fe(III)/PMS can generate multiple radicals ($SO_4^{\bullet-}$ and $^{\bullet}OH$) and non-radical Fe(IV). Fig. 3 depicts the Mo_2B_5 mediated direct route as an activator and indirect route as a co-catalyst for activating PMS *via* Fenton-like reaction. The universality of Mo_2B_5/Fe(III)/PMS for oxidizing multifold emerging contaminants (SIZ, diethyl phthalate (DEP), dimethyl phthalate (DMP), carbamazepine (CBZ), sulfamethoxazole (SMX), ibuprofen (IBP), benzoic acid (BA), bisphenol A (BPA), and phenol (PE)) with different molecular structures was further evaluated. $SO_4^{\bullet-}$ and $^{\bullet}OH$ typically engage with organic compounds through analogous reaction mechanisms, such as H atom abstraction, electron abstraction as well as radical addition [42]. Compared to $^{\bullet}OH$ (2.7 V), $SO_4^{\bullet-}$ not only has comparable oxidation potential (2.5–3.1 V) but also shows more significant selective oxidation properties for electron-rich contaminants [43]. $^{\bullet}OH$ is an unselective ROS for almost all of these contaminants (10^9–10^{10} L mol^{-1} s^{-1}) [44], while $SO_4^{\bullet-}$ exhibits comparatively lower reactivity toward DMP and DEP (6.4×10^7 L mol^{-1} s^{-1}) with reaction rates 2–3 orders of magnitude below those of $^{\bullet}OH$ [45]. Furthermore, Fe(IV) (2.0 V) exhibits selective reactivity towards electron-donating moieties in organic molecules, attributed to its intermediate oxidation potential and distinct reaction mechanisms, including oxygen atom transfer, hydride abstraction, and electrophilic addition [46].

Fig. 4a and Fig. S12 (Supporting information) show that Mo_2B_5/Fe(III)/PMS can completely degrade various organic pollutants within 15 min, while all three ROS are effective in degrading SMX, BA, CBZ, PE, IBP, SIZ and BPA based on results of quenching experiments. However, both TBA and MeOH significantly inhibited this system for degrading of DEP and DMP, suggesting that $^{\bullet}OH$ is the main ROS for oxidizing these highly refractory pollutants. Despite the strong inhibitory effects of TBA and MeOH, this system still shows high degradation efficiencies for other pollutants, which is attributed to the Fe(IV)-mediated non-radical pathway. The synergistic formation of $SO_4^{\bullet-}$, $^{\bullet}OH$, and Fe(IV) thus overcomes the limitations of a single ROS-dominated oxidation system. While $SO_4^{\bullet-}$ and $^{\bullet}OH$ excel in degrading a wide range of pollutants, Fe(IV) provided a complementary pathway for pollutants with complex structures. The substrate-dependent reactivity of Mo_2B_5/Fe(III)/PMS is further demonstrated by the significant variation in k_{obs} of different pollutants, and Fig. 4b shows a significant difference in k_{obs} for the oxidation of different organic pollutants (0.12–0.96 min^{-1}). Mo_2B_5/Fe(III)/PMS has relatively low oxidation capacity for refractory pollutants, and the k_{obs} values of DEP (0.12 min^{-1}) and DMP (0.12 min^{-1}) were relatively lower than those of the other seven pollutants (0.53–0.96 min^{-1}). These results indicate that Mo_2B_5/Fe(III)/PMS with the composite ROS can synergistically degrade various pollutants, which ensures the robust performance of the system across a wide range of pollutants.

The recovery of Fe(II) directly determines the efficiencies of Fenton-like systems, the conversion of iron species was thus investigated by monitoring the dynamics of various iron species (Fig. 5a). In Mo_2B_5/Fe(III)/PMS, the content of total dissolved iron was consistently maintained at 20 μmol/L (same as the initial Fe(III) dosage), indicating that no obvious iron ions precipitated on the surface of Mo_2B_5. Comparative experiments revealed rapid Fe(II) oxidation in Fe(II)/PMS, with 80 % conversion to Fe(III) occurring by 1 min and complete oxidation of Fe(II) achieved at 3 min. Meanwhile, Fe(III)/Mo_2B_5 exhibited markedly faster reduction kinetics, achieving complete Fe(III) reduction to form Fe(II) at 1 min. This stable Fe(II) generation process suggests that Mo_2B_5 can reduce Fe(III) on its surface by directly donating electrons. The regenerated Fe(II) was then released into the aqueous phase for initiating Fenton-like processes to generate ROS. This confirms that Mo_2B_5 can significantly accelerate the iron cycle *via* electron donation. Notably, Fe(II) was not identified in Mo_2B_5/Fe(III)/PMS system, and it is hypothesized that newly generated Fe(II) may be rapidly consumed by PMS. Moreover, solid-state EPR analysis revealed the presence of paramagnetic oxygen vacancy (OV) centers in the original Mo_2B_5 ($g = 2.004$, Fig. 5b). OVs can act as electron-rich regions to enhance the electron donation ability on the Mo_2B_5 surface. These results further confirmed that Mo_2B_5 as an excellent electron donor can provide electrons to directly activate PMS and indirectly accelerate iron-mediated Fenton-like reaction for producing ROS.

To elucidate the conformational relationship of electron transfer routes of Mo_2B_5 in Mo_2B_5/Fe(III)/PMS, the interfacial evolution of pristine and reacted Mo_2B_5 was systematically characterized using various surface analytical techniques. Full spectral analysis by XPS (Fig. 5c) showed that there was no dramatical change in the elemental species of the samples after reaction, with a relative enhancement of the intensity of the B 1s peaks in the post-reaction samples compared to the pre-reaction ones. In contrast, the intensity of the Mo 3d peak was reduced, which was closely related to

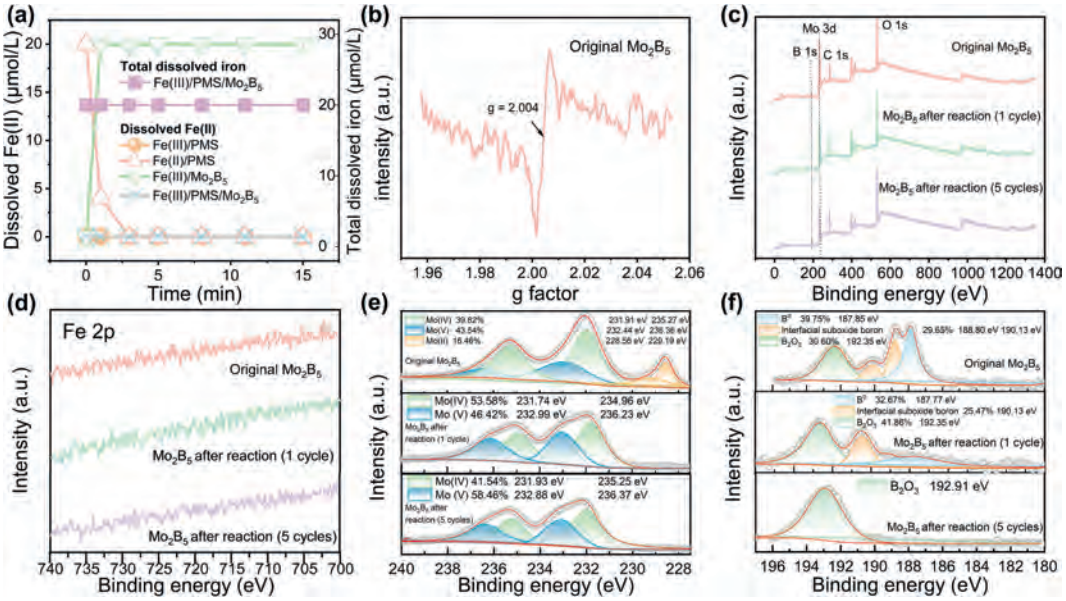


Fig. 5. Mechanism analysis. (a) Transformation of iron species, (b) EPR spectrum of original Mo_2B_5, (c) full XPS spectra and XPS spectrum of (d) Fe 2p, (e) Mo 3d, (f) B 1s of Mo_2B_5 before and after experiments.

the surface selective oxidation process. Meanwhile, Raman spectroscopic analysis revealed progressive attenuation of characteristic O-Mo-O vibrational modes at 191.2 cm^{-1} (antisymmetric stretching) and 332.3 cm^{-1} (symmetric stretching) with the increase in the number of reaction cycles (Fig. S13 in Supporting information) [47]. This indicates that the low-valent molybdenum in Mo_2B_5 was oxidized by PMS (for direct PMS activation) or Fe(III) (for indirect Fenton-like reaction), and the weakening of the Mo 3d peaks in the XPS spectra may result from the generation of a thick oxide layer on the Mo_2B_5 surface or the presence of multiple oxidation states (Mo(V) and Mo(VI)) [47]. Furthermore, Fe 2p XPS spectra in Fig. 5d shows that neither Fe(II) nor Fe(III) was detected on Mo_2B_5 surface both before and after experiments. This data confirms that after Fe(III) reduction on the Mo_2B_5 surface, the generated Fe(II) rapidly desorbs into the solution phase through the solid-liquid interfacial mass-transfer process, which in turn triggers homogeneous activation of PMS *via* Fenton-like reaction. This surface-body-phase synergistic mechanism avoids active site blockage and provides key experimental evidence for constructing a quasi-homogeneous Fenton-like system in dynamic equilibrium.

Quantitative analysis of Mo 3d spectra (Fig. 5e) showed that the low-valent Mo (Mo(II)) decreased from the initial 16.5 % to 0 % after one cycle, whereas Mo(IV) and Mo(V) increased from 39.8 % and 43.5 % to 53.6 % and 46.4 %, respectively; and Mo(IV) decreased to 41.5 % and Mo(V) increased to 58.5 % after five cycles. These confirm the role of *Mo species* as the main electron donor in Mo_2B_5/Fe(III)/PMS. The proportion of Mo in the low valence state is always maintained during the reaction cycle, which keeps its electron-donating ability and ensures the stability of its recycling. Moreover, the analysis of the chemical state evolution of elemental boron (Fig. 5f) revealed a significant structural reconfiguration. The pristine Mo_2B_5 particles readily react with oxygen to form a surface layer of low oxidized boron and boron oxide on the Mo_2B_5 particles. This surface oxidation process explains the relatively high interfacial suboxide boron and B_2O_3 detected at the interface. The share of monomeric boron (B^0, 187–188 eV) decreased from an initial 39.8 % to 32.9 % after one reaction cycle, whereas the B_2O_3 fraction (190–193 eV) correspondingly increased from 30.6 % to 41.9 %. This phenomenon indicates that Mo_2B_5 transfers electrons to Fe(III) as the reaction proceeds, and the chemical valence of boron gradually increased and was accompanied

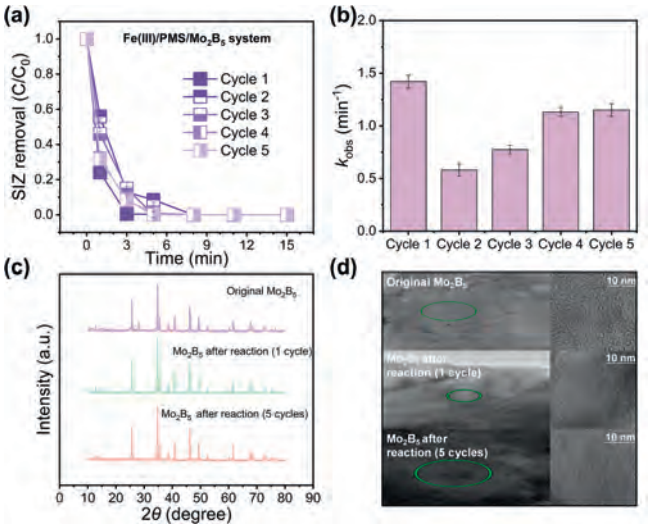


Fig. 6. Self-cleaning effect of Mo_2B_5 surface in the Mo_2B_5/Fe(III)/PMS system during cycling tests. (a) Curves and (b) k_{obs} of SIZ removal, (c) XRD spectra and (d) HRTEM images of Mo_2B_5.

by the production of intermediate oxides and B_2O_3. In addition, FT-IR spectroscopy showed that Mo_2B_5 underwent surface oxidation and hydrolysis to produce B-OH, with a slight enhancement of both B-O and Mo-O peaks during the reaction in Mo_2B_5/Fe(III)/PMS (Fig. S14 in Supporting information).

Cyclic stability tests (Fig. 6a) revealed that Mo_2B_5 exhibited excellent and high stable co-catalysis performance, the Mo_2B_5/Fe(III)/PMS system consistently maintained efficient degradation kinetics for SIZ. This system could still achieve the complete degradation of SIZ within 8 min in cycle 5, which fully demonstrated the excellent stability and reusability of the co-catalytic system for the deep treatment of organic pollutants. In addition, the values of k_{obs} exhibited an atypical enhancement over 5 consecutive cycles (Fig. 6b), contrasting sharply with conventional Fenton-like systems that typically suffer from rapid activity decay. Characterization of XRD and HRTEM explained this phenomenon and revealed the surface reconstruction process caused by cycling

tests (Figs. 6c and d). As shown in Fig. 6c, after several rounds of oxidation reaction in Mo_2B_5/Fe(III)/PMS, the characteristic diffraction peaks of Mo_2B_5 did not show any obvious displacement or intensity attenuation, and the characteristic peaks of heterogeneous phases were not detected. This structural characterization result confirms the remarkable structural stability of Mo_2B_5 in Mo_2B_5/Fe(III)/PMS from the crystallographic level. This excellent lattice integrity provides an important guarantee for the long-lasting operation of Mo_2B_5 and also explains the microscopic mechanism by which the system can maintain stable oxidation capability. Moreover, HRTEM images in Fig. 6d depicts that the pristine Mo_2B_5 exhibits typical crystal structure features, and the amorphous structure appears in local regions on Mo_2B_5 surface after 5 cycles. Although the formation of the surface amorphous layer was observed, there was no significant increase in the half-peak widths of the characteristic peaks in the XRD spectra (Fig. 6c), indicating that the amorphous layer was limited to the surface and the bulk structure remained intact. In addition, cyclic experiments confirmed that the amorphous layer has no significant negative impact on long-term catalytic activity. This is due to the fact that the B and Mo atoms on the Mo_2B_5 surface will be converted to ions resulting from the availability of electrons during direct and indirect routes for PMS activation, and meanwhile, the Mo_2B_5 surface can be renewed. This dynamic equilibrium phenomenon of the surface interface structure reveals a unique self-renewal mechanism of Mo_2B_5. ICP-MS analysis (Fig. S15 in Supporting information) shows the relatively low leaching concentrations of Mo (1.4 and 1.8 mg/L) and boron (1.2 and 1.4 mg/L) after 1 cycle test and 5 cycle tests, respectively, and the atom ratio of Mo to B was around 1.25 (Mo/B). The controlled decomposition of the reductive sites on the Mo_2B_5 surface not only effectively avoids the accumulation of catalytically toxic substances, but also achieves *in-situ* regeneration of the active sites by the exposure of fresh internal crystalline surfaces. Therefore, oxidation etching preferentially removed the passivation layer on the Mo_2B_5 surface for exposing more inside active sites, resulting in high co-catalytic performance in the cyclic tests.

In conclusion, we found that Mo_2B_5 as an efficient and multifunctional co-catalyst exhibited excellent enhancement in assisting Fenton-like system (Mo_2B_5/Fe(III)/PMS) by virtue of its unique dual-active-site configuration and metal-like electron-conducting property. Mo_2B_5 can enhance the activation of PMS through dual pathways: (1) Direct activating PMS to generate $^{\bullet}OH$; (2) indirect activating PMS to produce $SO_4^{\bullet-}$ and Fe(IV) *via* Fenton-like reaction by low valent species of boron and molybdenum induced Fe(III) reduction. Due to the production of these ROS, the Mo_2B_5/Fe(III)/PMS system exhibits broad-spectrum oxidative capacity toward diverse organic contaminants *via* synergetic radical and non-radical routes. Moreover, the unique self-renewal mechanism of Mo_2B_5 ensures its long-lasting stability for co-catalyzing Fenton-like reaction during long-term operation. Therefore, this work provides a sustainable paradigm for water remediation by integrating dual co-catalytic pathways and developing a high-performance Fenton-like technology.

Declaration of competing interest

The authors declare that they have no known competing financial interests or personal relationships that could have appeared to influence the work reported in this paper.

CRediT authorship contribution statement

Xinyun Zhang: Writing – review & editing, Writing – original draft, Investigation, Formal analysis, Data curation. **Chenying Zhou:** Investigation, Formal analysis, Data curation. **Jian Zhang:** Project administration, Formal analysis. **Minglu Sun:** Writing – review & editing, Supervision, Investigation, Formal analysis, Data curation. **Yanbiao Shi:** Supervision, Funding acquisition. **Chuanshu He:** Supervision, Formal analysis. **Xiaowei Huo:** Supervision, Formal analysis. **Yang Liu:** Supervision. **Peng Zhou:** Writing – review & editing, Writing – original draft, Supervision, Investigation, Formal analysis. **Bo Lai:** Writing – review & editing, Supervision, Project administration, Funding acquisition.

Acknowledgments

This research was supported financially by National Natural Science Foundation of China (Nos. U24A20561 and 22306119), Sichuan Science and Technology Program (No. 2024NSFTD0014) and Key R&D Program of Heilongjiang Province (No. 2023ZX02C01).

Supplementary materials

Supplementary material associated with this article can be found, in the online version, at doi:10.1016/j.cclet.2025.111630.

References

[1] A. Shokri, M.S. Fard, Environ. Chall. 7 (2022) 100534.
[2] X. Li, D. Wu, T. Hua, et al., Sci. Total Environ. 804 (2022) 150096.
[3] X. Zhou, X. Li, Y. Xiang, et al., Chin. Chem. Lett. 36 (2025) 110664.
[4] Z. Li, L. Wang, Y. Liu, et al., Water Res. 168 (2020) 115093.
[5] S. Xiao, M. Cheng, H. Zhong, et al., Chem. Eng. J. 384 (2020) 123265.
[6] J. Guo, B. Gao, Q. Li, et al., Adv. Mater. 36 (2024) 2403965.
[7] S. Meng, M. Sun, P. Zhang, et al., Environ. Sci. Technol. 57 (2023) 12534–12545.
[8] Z. Yang, C. Shan, B. Pan, et al., Environ. Sci. Technol. 55 (2021) 8299–8308.
[9] T. Li, Z. Zhao, Q. Wang, et al., Water Res. 105 (2016) 479–486.
[10] X. Li, Y. Liu, J. Wei, et al., Chin. Chem. Lett. 36 (2025) 110811.
[11] P. Zhou, W. Ren, G. Nie, et al., Angew. Chem. Int. Ed. 132 (2020) 16517–16526.
[12] M. Huang, X. Wang, C. Liu, et al., J. Hazard. Mater. 404 (2021) 124175.
[13] J. Guo, Y. Wang, Y.A. Shang, et al., Proc. Natl. Acad. Sci. U. S. A. 121 (2024) e2313387121.
[14] Y. Chen, R. Su, F. Xu, et al., J. Hazard. Mater. 470 (2024) 134162.
[15] X. Liu, Y. Gong, Inorg. Chem. 60 (2021) 18075–18081.
[16] H. Schaefer, F. Harris, Phys. Rev. 167 (1968) 67–73.
[17] B. Albert, H. Hillebrecht, Angew. Chem. Int. Ed. 48 (2009) 8640–8668.
[18] P. Zhou, S. Meng, M. Sun, et al., Sep. Purif. Technol. 317 (2023) 123860.
[19] M. Xing, W. Xu, C. Dong, et al., Chem 4 (2018) 1359–1372.
[20] X. Liu, Q. Jia, S. Zhang, et al., Int. Mater. Rev. 69 (2024) 107–141.
[21] X. Duan, W. Li, Z. Ao, et al., J. Mater. Chem. A 7 (2019) 23904–23913.
[22] Z. Wang, W. Qiu, S. Pang, et al., Chem. Eng. J. 371 (2019) 842–847.
[23] K. Yu, L. Li, C. Zang, et al., Colloid. Surf. A 578 (2019) 123607.
[24] P. Shao, X. Duan, J. Xu, et al., J. Hazard. Mater. 322 (2017) 532–539.
[25] J. Zou, J. Ma, L. Chen, et al., Environ. Sci. Technol. 47 (2013) 11685–11691.
[26] Y. Peng, G. Xie, P. Shao, et al., Appl. Catal. B: Environ. 310 (2022) 121345.
[27] J. Espinosa, S. Navalón, M. Álvaro, et al., ChemCatChem 8 (2016) 2642–2648.
[28] H. Cheng, H. Liu, C. Huang, et al., Sep. Purif. Technol. 330 (2024) 125311.
[29] X. Zhang, J. Wang, Y. Wang, et al., J. Hazard. Mater. 442 (2023) 130115.
[30] J. Lin, W. Tian, Z. Guan, et al., Adv. Funct. Mater. 32 (2022) 2201743.
[31] M. Li, K. Zheng, Y. Jin, et al., J. Mater. Sci. Technol. 137 (2023) 67–78.
[32] R. Hirani, A. Asif, N. Rafique, et al., Sep. Purif. Technol. 319 (2023) 124110.
[33] F. Ghanbari, M. Moradi, Chem. Eng. J. 310 (2017) 41–62.
[34] C. Cheng, W. Ren, F. Miao, et al., Angew. Chem. Int. Ed. 62 (2023) e202218510.
[35] E. Braxton, D. Fox, B. Breeze, et al., ACS Measur. Sci. Au 3 (2023) 21–31.
[36] M. Cashman, L. Kirschenbaum, J. Holowachuk, et al., J. Hazard. Mater. 380 (2019) 120875.
[37] G. Buxton, C. Greenstock, W. Helman, et al., J. Phys. Chem. Ref. Data 17 (1988) 513–886.
[38] P. Neta, R. Huie, A. Ross, J. Phys. Chem. Ref. Data 17 (1988) 1027–1284.
[39] Z. Wang, W. Qiu, S. Pang, et al., Environ. Sci. Technol. 56 (2022) 1492–1509.
[40] Z. Wang, J. Jiang, S. Pang, et al., Environ. Sci. Technol. 52 (2018) 11276–11284.
[41] H. Dong, Y. Li, S. Wang, et al., Environ. Sci. Technol. Lett. 7 (2020) 219–224.
[42] U. Hübner, S. Spahr, H. Lutze, et al., Heliyon 10 (2024) e30402.
[43] M. Zhang, J. Ruan, X. Wang, et al., Water Res. 246 (2023) 120697.
[44] P. Zhou, Y. Yang, W. Ren, et al., Appl. Catal. B: Environ. 319 (2022) 121916.
[45] R. Xiao, T. Ye, Z. Wei, et al., Environ. Sci. Technol. 49 (2015) 13394–13402.
[46] C. Zhang, W. Zuo, L. Ai, et al., J. Colloid. Interf. Sci. 669 (2024) 794–803.
[47] J. Baltrusaitis, B. Mendoza-Sanchez, V. Fernandez, et al., Appl. Surf. Sci. 326 (2015) 151–161.